coatings

MDPI

Article

Plasma Etching Behavior of YOF Coating Deposited by Suspension Plasma Spraying in Inductively Coupled CHF_3/Ar Plasma

Seungjun Lee, Jaehoo Lee, Woongsik Kim * and Nong-Moon Hwang *

Department of Materials Science and Engineering, Seoul National University, Seoul 08826, Korea; lsj2914@snu.ac.kr (S.L.); caspiel5202@snu.ac.kr (J.L.)

* Correspondence: woongs1@snu.ac.kr (W.K.); nmhwang@snu.ac.kr (N.-M.H.)

Received: 9 September 2020; Accepted: 23 October 2020; Published: 24 October 2020

Abstract: Dense yttrium oxyfluoride (YOF) coating was successfully deposited by suspension plasma spraying (SPS) with coaxial feeding. After deposition for 6 min at a plasma power of 105 kW, the thickness of the YOF coating was 55 ± 3.2 μm with a porosity of 0.15% ± 0.01% and the coating rate was ~9.2 μm/min. The crystalline structure of trigonal YOF was confirmed by X-ray diffractometry (XRD). The etching behavior of the YOF coating was studied using inductively coupled CHF_3/Ar plasma in comparison with those of the Al_2O_3 bulk and Y_2O_3 coating. Crater-like erosion sites and cavities were formed on the whole surface of the Al_2O_3 bulk and Y_2O_3 coating. In contrast, the surface of the YOF coating showed no noticeable difference before and after exposure to the CHF_3/Ar plasma. Such high resistance of the YOF coating to fluorocarbon plasma comes from the strongly fluorinated layer on the surface. The fluorination on the surface of materials was confirmed by X-ray photoelectron spectrum analysis (XPS). Depth profiles of the compositions of Al_2O_3, Y_2O_3, and YOF samples by XPS revealed that the fluorination layer of the YOF coating was much thicker than those of Al_2O_3 and Y_2O_3. These results indicate that if the inner wall of the semiconductor process chamber is coated by YOF using SPS, the generation of contamination particles would be minimized during the fluorocarbon plasma etching process.

Keywords: fluorocarbon plasma; etching; yttrium oxyfluoride (YOF); plasma-resistant material; suspension plasma spraying (SPS); X-ray photoelectron spectrum (XPS)

1. Introduction

In the semiconductor manufacturing process, dry etching of dielectric SiO_2 and cleaning processes have increased due to multi-level interface connections [1]. Moreover, recently, as the incorporation of integrated circuits on wafers reaches its limit, three-dimensional vertical NAND (3D V NAND) technology, which stacks circuits in multi-layers, has been introduced and thereby the dry etching process is repeated many times in a chamber. As fluorocarbon plasma gases such as CF_4, CHF_3, and C_2F_6 are typically used in the process, the inner wall of the chamber is exposed to those corrosive gases [2]. These fluorocarbon gases tend to etch the materials of the inner wall. As a result, many contamination particles are generated and the etching causes a process drift phenomenon [3]. These phenomena cause fatal problems such as a decrease in yield during mass production and the reduced operating efficiency of machines [4]. In order to prevent the etching phenomena, SiO_2 and Al_2O_3 are used as plasma-resistant materials of the inner wall of the chamber. However, they turn out to become vulnerable to the fluorocarbon plasma gases as the number of drying etching cycles increases [1,5–8]. Recently, Y_2O_3, which is more chemically stable to the fluorocarbon plasma than Al_2O_3 and SiO_2, has been used as a plasma-resistant material [9]. When Y_2O_3 coating is exposed to fluorocarbon

plasma, a fluorinated layer forms on its surface [9,10]. The fluorinated layer acts as a protective layer which prevents the coating from reacting with the fluorocarbon plasma [9]. Although Y_2O_3 is known to be more resistant to plasma than SiO_2 and Al_2O_3, it would not be the best plasma-resistant material because fluoride particles whose chemical composition is close to YF_3 are generated as contaminants in the process of the Y_2O_3 surface being converted to a $Y_xO_yF_z$ layer, due to the reaction with plasma [11,12]. Nowadays, many researchers are paying attention to the $Y_xO_yF_z$ (YOF) layer formed on the surface of the Y_2O_3. Since yttrium oxyfluoride (YOF) contains fluorine, it would not react with the fluorocarbon plasma gas. Shiba et al. [9] reported that the surface crystallinity of YOF, which is a fluorine-based material, was not changed, while that of Y_2O_3 was changed by the penetration and reaction with fluorocarbon plasma gas. YOF has metal and oxide compositions which are chemically stable, so particle generation would also be suppressed [9,13]. Shiba et al. [9] also reported that the resistance to erosion of YOF for various plasma gases was superior to that of Y_2O_3 through X-ray diffractometry (XRD) and X-ray photoelectron spectrum (XPS) analyses, although those materials were deposited by ion plating. Since atmospheric plasma spraying (APS) is more cost effective and suitable for coating large areas than ion plating, it is widely used in coating plasma resistant materials. Although APS can produce a thick coating on a large area with high efficiency, numerous cracks and pores tend to be formed in the coating and thereby the coating is vulnerable to plasma erosion. If suspension plasma spraying (SPS) is used, a dense coating free of cracks can be deposited. This is because relatively fine particles less than 5 μm in size can be dispersed in the suspension, and the splat size of the coating layer is sufficiently small. Considering that SPS is such a promising coating method, it is worth depositing the YOF coating by SPS and analyzing its plasma-resistant properties. However, there have only been a few reports about dense YOF coating deposited by SPS and its plasma-resistant properties. Recently, a dense YOF coating was successfully deposited by SPS by our group [11]. Our previous paper focused on the optimum process conditions to deposit a dense coating by SPS. In this paper, the plasma-resistant properties of the YOF coatings were analyzed in comparison with those of Al_2O_3 bulk and Y_2O_3 coating. After exposing these materials to fluorocarbon plasma, the surface and internal compositions were analyzed by XPS, and the crystalline structures were analyzed by XRD.

2. Experimental Procedures

Commercially available $Y_5O_4F_7$ suspension (Nippon Yttrium Co., Ltd., Omuta, Fukuoka, Japan), which consists of $Y_5O_4F_7$ particles with an average size of 3 μm dispersed in deionized water with a solid concentration of 10 wt.%, was used as a feedstock material. A YOF coating was prepared using a suspension plasma spraying (SPS) system, which had triple anodes and cathodes with coaxial feeding (Mettech's Axial III, Northwest Mettech Corp., North Vancouver, BC, Canada). A plate of Al alloy 6061 (50 mm × 50 mm × 10 mm) was used as a substrate.

To improve the adhesion strength of the YOF coating, the substrate was sandblasted to have a surface roughness average (*R*a) of ~2.8 μm by alumina particles less than 254 μm in size. The Al alloy substrate was preheated with the plasma flame before the SPS coating process. The temperature of the substrate was found to be ~380 K after the substrate was preheated, and was measured to be ~550 K by a pyrometer (568 IR thermometer, Fluke, Washington, USA) after SPS coating. During the SPS process, the substrate was cooled by an air gun at a distance of 100 cm to prevent the substrate from melting in the high-temperature plasma flame. The axial III SPS system with axial feeding has a higher coating efficiency than other SPS systems with radial feeding.

As shown in Figure 1, the suspension flows directly through the plasma jet and thereby the heat generated from the plasma jet transfers efficiently to the suspension. The SPS coating was carried out under the following conditions; the flow rate of argon as a primary gas was set to 90 standard liters per minute (slm), and the flow rates of nitrogen and hydrogen as secondary gases were set to 54 and 36 slm, respectively, to induce the generation of a plasma arc with an arc current of 230 A. The role of gases is illustrated in our previous paper [11]. The feeding rate of the suspension was

45 standard cubic centimeters per minute (sccm), and the flow rate of nitrogen atomizing gas was 30 sccm. The atomizing gas, which is injected to the feeding flow and splits the suspension droplets into small ones, turned out to affect the quality of the YOF coating because it made the droplet size of the suspension smaller and thus, the particles in the droplet melted more easily [14,15]. The transverse speed of the plasma gun was 1000 mm/s, and coating cycles were repeated 20 times during the entire spraying process. The stand-off distance was 50 mm, which refers to the distance between the plasma gun and Al substrate. The details of the processing parameters of the YOF coating are shown in Table 1. The thickness of the YOF coating was about 55 µm, and the surface was polished to less than 0.1 µm of roughness for the test of fluorocarbon plasma etching. Polycrystalline Al_2O_3 bulk and Y_2O_3 coating deposited by SPS were prepared as a comparison group to investigate the etching behavior of the YOF coating and were polished to less than 0.1 µm surface roughness.

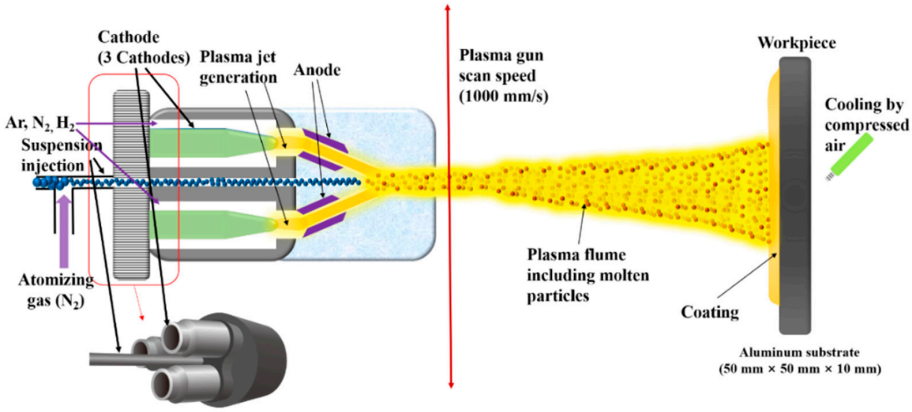

Figure 1. Schematic of the Axial III suspension plasma spray (SPS) system [14].

Table 1. Processing parameters for coatings made of yttrium oxyfluoride (YOF) by SPS.

Parameters	Conditions
Electric power (kW)	105
$Ar/N_2/H_2$ flow rate (slm)	90/54/36 (5:3:2 ratio)
Total gas flow rate (slm)	180
Arc current (A)	230
Feeding rate (sccm)	45
Atomizing gas flow rate (slm)	30
Stand Off Distance (mm)	50
Transverse speed (mm/s)	1000
Scan time (coating cycles)	20
Coating process time (min)	6

The plasma etching process was carried out by an inductively coupled plasma (ICP) etcher (Multiplex ICP, Surface Technology Systems (STS), Newport, UK) with the gases CHF_3 and Ar. Figure 2 shows a schematic of the STS multiplex ICP system. The YOF coating, Y_2O_3 coating, and Al_2O_3 bulk specimens were placed on a silicon wafer and loaded into the ICP etching chamber to compare their etching behavior using fluorocarbon plasma. The mixture of CHF_3 and Ar gases was injected into the ICP etching chamber for plasma generation, and the gases were supplied at a 6:1 ratio of 50 and 8.3 sccm, respectively, through a gas inlet. Helium gas was used to cool the specimens on the wafer to prevent thermal damage during the etching process and was injected into the gas inlet under the electrostatic chuck (ESC). The RF source power and bias power were set to 2100 and 210 W, respectively, which were 70% of the maximum allowable values of the ICP etching chamber (3000, 300 W). Dry and turbo molecular pumps were utilized to prepare the vacuum. The working pressure in the plasma etching chamber was 20 mTorr. The specimens were exposed to CHF_3/Ar plasma for 60 min. The details of the plasma etching conditions are shown in Table 2.

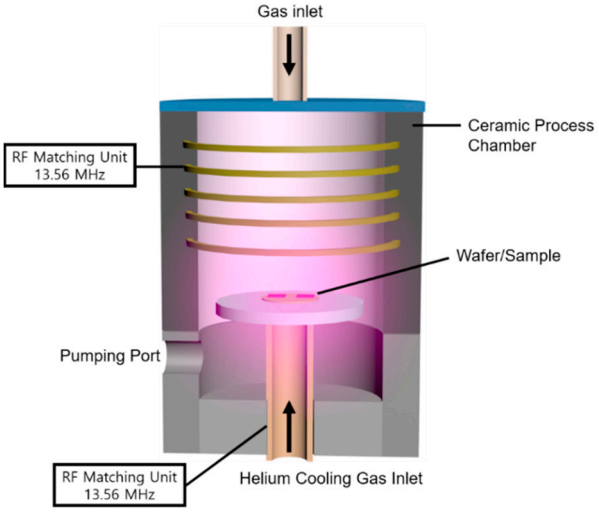

Figure 2. Schematic of the Surface Technology Systems (STS) multiplex inductively coupled plasma (ICP) system.

Table 2. Details of the plasma etching conditions of the ICP system.

Parameters	Conditions
RF Source power (W)	2100
RF Bias power (W)	210
Pressure (mTorr)	20
Gas flow of CHF_3:Ar (SCCM)	50:8.3 (6:1 ratio)
He pressure (Torr)	9.5
He flow (SCCM)	15.6
Etching time (min)	60

The microstructures and surface morphologies were observed by field emission scanning electron microscopy (FE-SEM, SU-70, Hitachi, Tokyo, Japan) to analyze erosion behavior after fluorocarbon plasma etching. The crystal structure of the YOF coating by the SPS process was analyzed by high-resolution X-ray diffractometry (HR-XRD, SmartLab, Rigaku, Austin, TX, USA). In order to analyze the porosity of the cross-section of the YOF coating, an image analyzing program (ImageJ software (version 1.51k)) was used [16]. The hardness of the YOF coating was measured by a Vickers hardness tester (Duramin-40, Struers, Cleveland, USA) under a load of 200 gf. The etching depth of the specimens was measured by a noncontact three-dimensional surface profiler (NanoView-E1000, NanoSystem, Daejeon, Korea). High-resolution X-ray photoelectron spectrum (HR-XPS, AXIS SUPRA, Kratos, Manchester, UK) analysis was carried out by a monochromatic Al Kα X-ray source at a passing energy of 20 eV with a 700 µm × 400 µm spot size. The deconvolution of the photoelectron spectrum was performed by using a fitting program (Fitt-win software (version 1.3)) to analyze the spectrum of the core energy levels of the Y3*d* and Al2*p* states from the surface of YOF and Al_2O_3 after exposure to fluorocarbon plasma. In order to investigate the chemical compositions, depth profiling was performed with focused Ar^+ ions for sputtering of the etched surface of the Al_2O_3 bulk, Y_2O_3 coating, and YOF coating.

3. Results and Discussion

Figure 3 shows FE-SEM images of the surface and cross-section microstructures of the YOF coating deposited under the SPS conditions in Table 1. The FE-SEM image of the as-coated YOF surface morphology in Figure 3a shows both smooth and rough areas. After the solvent of the droplets coming out from the torch outlet is evaporated, the remaining particles will be melted by the plasma flame.

The completely melted particles will be spread out onto a growing surface and produce smooth areas called splats [17]. The partially or incompletely melted particles produce rough areas.

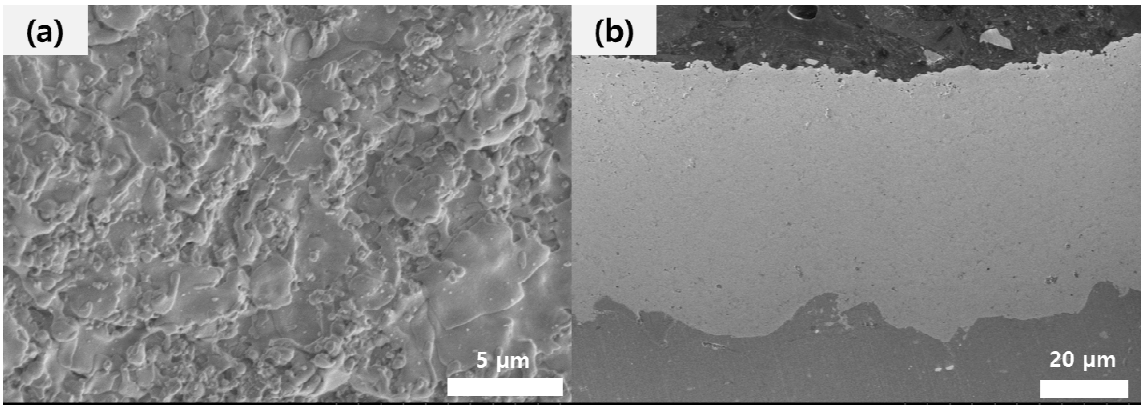

Figure 3. FE-SEM images of (**a**) the surface and (**b**) cross-section of the YOF coating deposited by the SPS process.

The pores observed on the cross-section in Figure 3b came from partial or incomplete melting [15]. The porosity was 0.15% ± 0.01%, which was calculated by the image analyzing program and determined by averaging five randomly selected areas from the entire area of coating. The thickness of the YOF coating in Figure 3b was 55 ± 3.2 μm and the coating rate was ~9.2 μm/min. The porosity of the YOF coating affects its hardness. The Vickers hardness of the YOF coating in Figure 3 was 553 ± 60 HV, which is much higher than 290 ± 30 HV for the YOF coating deposited by atmospheric plasma spraying (APS) reported recently by Lin et al. [18] and 69.34 ± 4 HV (0.68 ± 0.04 GPa) for the YOF coating fabricated by hot pressing reported by Tsunoura et al. [10].

Figure 4 shows the XRD peaks of the YOF coating. The major peaks indicated by the reverse triangles in Figure 4 represent the crystalline structure of trigonal YOF. The minor peaks indicated by squares and rhombuses represent, respectively, the crystalline phases of cubic and monoclinic Y_2O_3. Although cubic and monoclinic Y_2O_3 are unwanted phases, their formation was unavoidable to a certain extent. A possible scenario for the formation of Y_2O_3 would be as follows. First, $Y_5O_4F_7$ particles in suspension would be transformed into YOF particles, while $Y_5O_4F_7$ particles volatilize in the form of YF_3 in the plasma jet region [19]. Then, some of the YOF would be transformed into Y_2O_3, while the YOF is mainly volatilized in the form of YF_3 by sufficient heat energy in the plasma jet region [20]. The detailed mechanism is explained in our previous paper [11].

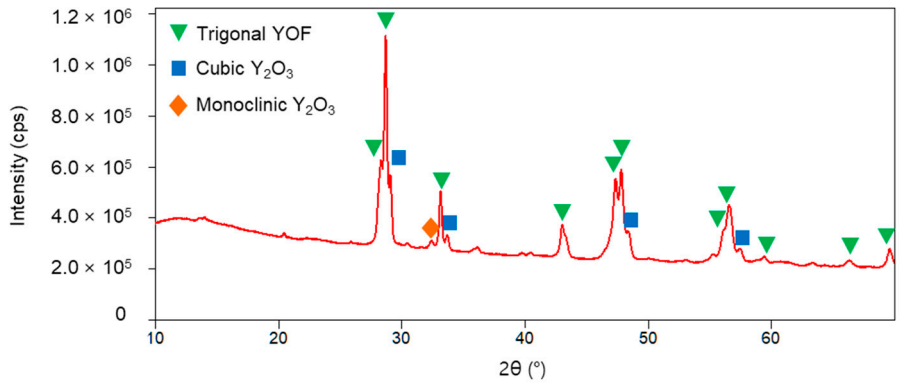

Figure 4. XRD patterns of the YOF coating deposited on the Al substrate by SPS.

Figure 5 shows the FE-SEM images of the surface microstructure of the Al_2O_3 bulk, Y_2O_3 coating, and YOF coating before and after exposure to the CHF_3/Ar plasma for 60 min. The Al_2O_3, Y_2O_3

coating, and YOF coating were polished to less than 0.1 μm of roughness, respectively. Furthermore, as shown in Figure 5a,c,e, they had a smooth surface before plasma exposure. After exposure to the fluorocarbon plasma, the erosion on the surface of the Al_2O_3 bulk was much more severe than that of the Y_2O_3 coating and the YOF coating. As shown in Figure 5b, large and small crater-like erosion sites were generated and contamination particles, which are shown as tiny dots in the figure, were observed on the Al_2O_3 surface after exposure to fluorocarbon plasma. As shown in Figure 5d, although the Y_2O_3 coating showed much less erosion than the Al_2O_3 bulk, it had more cavities and deeper erosion than the YOF coating.

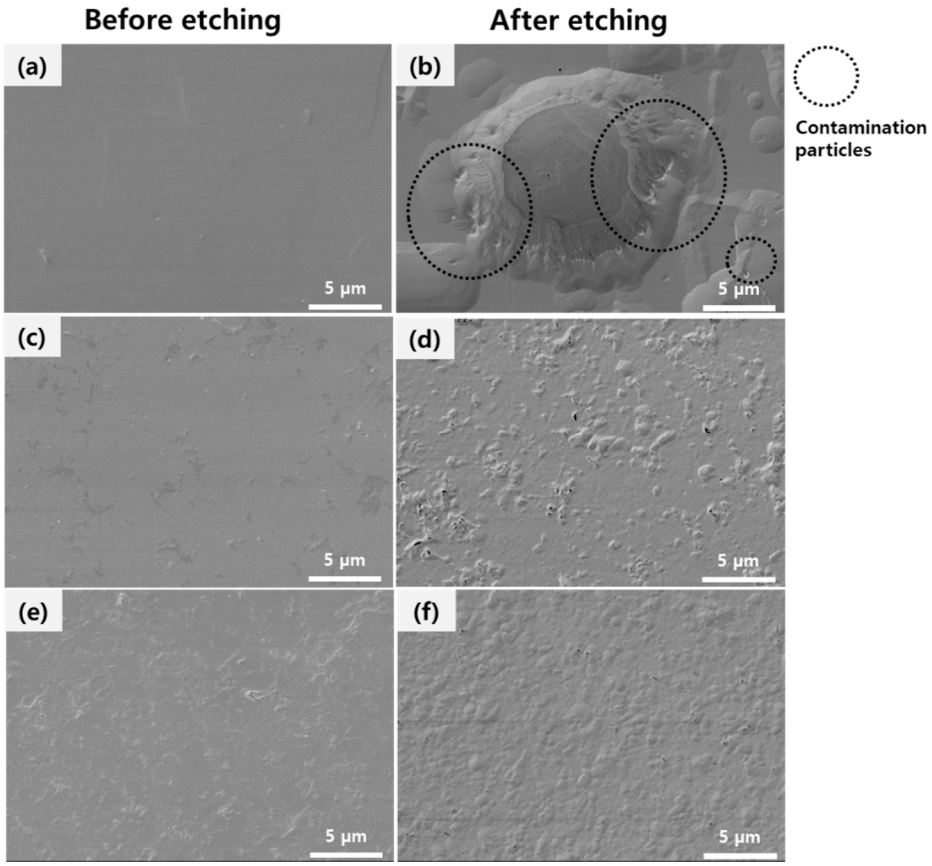

Figure 5. FE-SEM images of the polished surface of (**a**) Al_2O_3, (**c**) Y_2O_3 coating, and (**e**) YOF coating before plasma etching, and (**b**) Al_2O_3, (**d**) Y_2O_3 coating, and (**f**) YOF coating after plasma etching for 60 min.

As shown in Figure 5f, there was no noticeable difference in the surface of the YOF coating before and after exposure to the fluorocarbon plasma in comparison with those of the Al_2O_3 bulk and Y_2O_3 coating. Contamination particles were not observed. Although both the Y_2O_3 and YOF coatings were deposited by the SPS process under the same conditions, the YOF coating showed less erosion, which means that YOF is chemically more stable than Y_2O_3 against fluoride etching species, which is in agreement with the previous report by Yoshinobu et al. [5].

On the other hand, the plasma resistance of the YOF coating is closely related to its densification because the internal pores within the grains or at grain boundaries tend to be intensively eroded from their edges, forming crater-like erosion sites [21]. The crater-like erosion sites formed from internal pores were barely observed in Figure 5f, which would be due to the low porosity of 0.15% ± 0.01% of the YOF coating deposited by SPS with a uniaxial feeding system. Hence, in addition to the chemical stability of the YOF coating, it is further necessary to reduce the porosity of the YOF coating to improve its plasma resistance. The SPS process is suitable for reducing the porosity of the YOF coating.

Figure 6 shows the etched depth of the Al_2O_3, Y_2O_3, and YOF surfaces with the plasma exposure time. The etched depth was measured in nine areas of their surfaces and the average value was calculated. The etched depth of the Al_2O_3 surface steeply increased after 30 min in comparison with that of the Y_2O_3 and YOF surfaces and became more than 1025 nm after 60 min. As plasma etching progressed, crater-like erosion sites were formed. Once they were formed, the erosion seemed to be accelerated, spreading from the erosion sites as shown in Figure 6. On the other hand, the etched depths of the Y_2O_3 and YOF surfaces were, respectively, 289 and 142 nm after 60 min of plasma exposure and increased almost linearly with the plasma exposure time. Considering that the Al_2O_3, Y_2O_3, and YOF surfaces were equally bombarded by ions of Ar plasma in the presence of highly corrosive fluorocarbon [13], the difference in the etched depth of the three samples in Figure 6 means that the YOF coating is more resistant to the CHF_3 plasma than the Y_2O_3 coating, which is more resistant than the Al_2O_3 bulk.

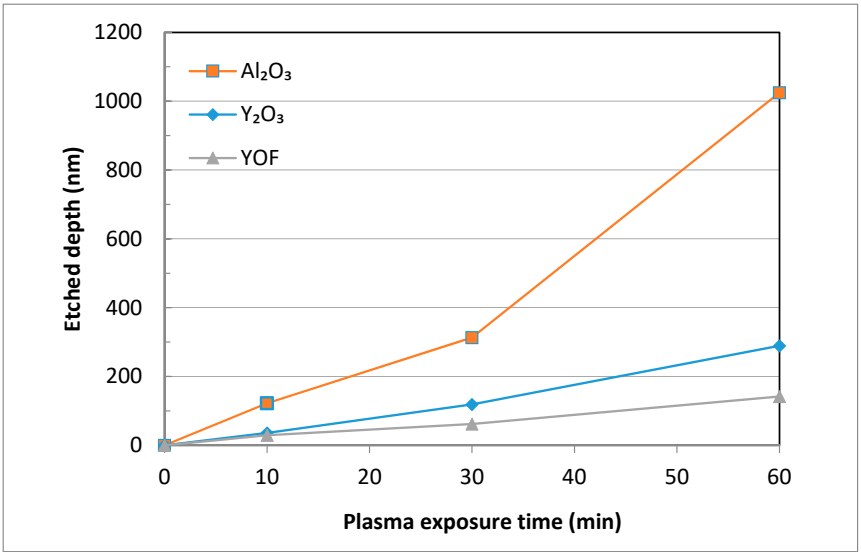

Figure 6. Etched depth of Al_2O_3 bulk, Y_2O_3, and YOF coatings deposited by SPS as a function of the exposure time of CHF_3/Ar plasma.

Figure 7 shows the XPS spectra of the Al_2O_3, Y_2O_3, and YOF surfaces after 60 min of CHF_3/Ar plasma etching. The peak separation of XPS spectra of the three samples indicated that their surfaces were obviously fluorinated. The XPS spectra of the fluorinated surfaces, which are shown by the dotted lines in Figure 7, were fitted to two doublets, which are shown by the dashed and long dashed lines.

In Figure 7a of Al_2O_3 bulk, the two doublets of Al atoms from Al_2O_3 are Al2$p_{3/2}$ and Al2$p_{1/2}$ peaks, which represent 3/2 and 1/2 spins of the 2*p* orbital, respectively. It is reported in the handbook of XPS standards [22] that the peaks have an intensity ratio of 2:1 and peak position spacing in the binding energy of 0.4 eV. The two peaks of Al2$p_{3/2}$ were located at 75.0 and 76.2 eV. The peak of lower binding energy of 75.0 eV would be for Al–O bonding of pure Al_2O_3 [23,24]. The peak at the higher binding energy of 76.2 eV would be for Al–F bonding, which was also confirmed by the peak of F1*s* located at 686.2 eV in the XPS spectrum of fluorine bonding [22].

On the other hand, the XPS spectra of Y atoms from the Y_2O_3 and YOF coatings with two doublets in Figure 7b,c consist of Y3$d_{5/2}$ and Y3$d_{3/2}$ peaks, respectively. The two peaks have an intensity ratio of 3:2 and peak position spacing in the binding energy of 2.05 eV [25]. The peaks of the lower binding energies of Y3$d_{5/2}$ and Y3$d_{3/2}$ from Y_2O_3 coating were located at 157.10 and 159.15 eV, and those of the higher binding energies of Y3$d_{5/2}$ and Y3$d_{3/2}$ were located at 159.40 and 161.45 eV in Figure 7b. The peaks at the lower binding energies at 157.10 and 159.15 eV correspond to the Y–O bonding, and those at the higher binding energies at 159.40 and 161.45 eV correspond to the Y–F bonding.

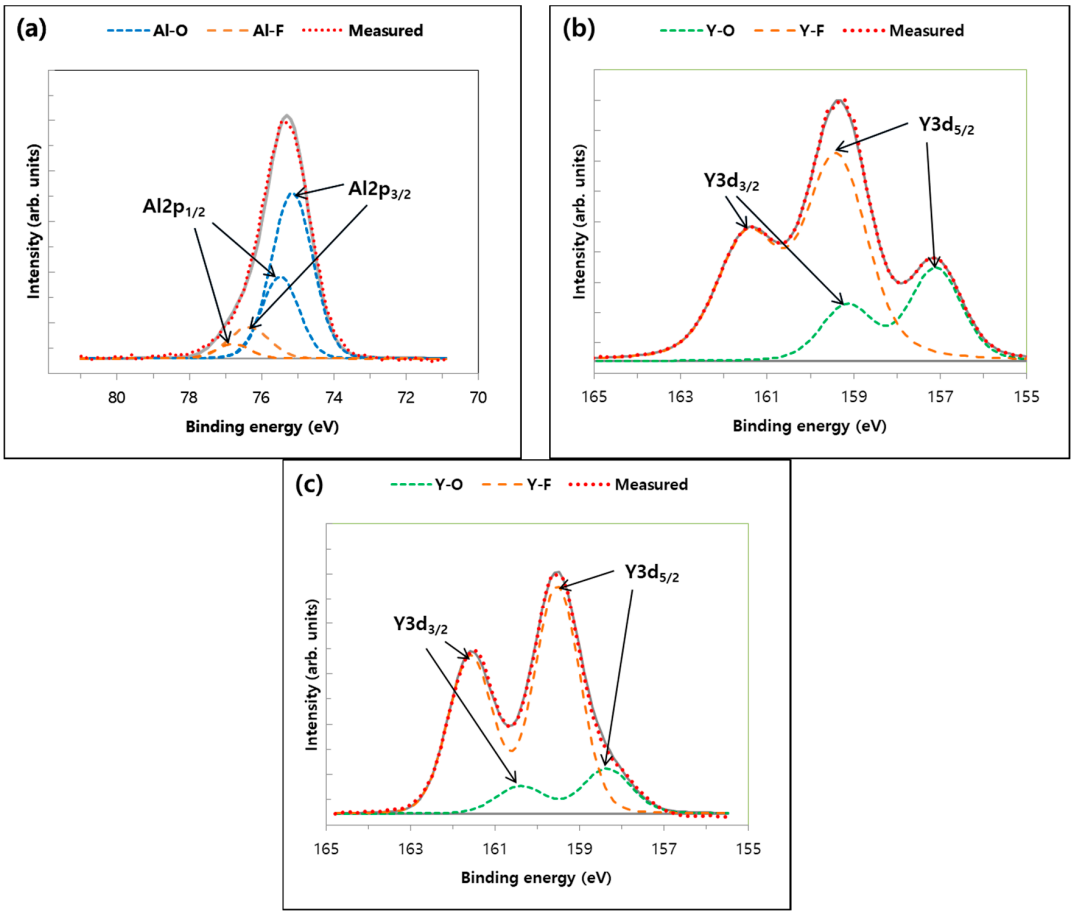

Figure 7. High-resolution X-ray photoelectron spectra of (**a**) Al from the surface of Al_2O_3, (**b**) Y from the surface of the Y_2O_3 coating, and (**c**) Y from the surface of the YOF coating after exposure to CHF_3/Ar plasma for 60 min.

In Figure 7c of the YOF coating, the peaks at the lower binding energies of Y3$d_{5/2}$ and Y3$d_{3/2}$ at 158.35 and 160.40 eV correspond to the Y–O bonding, and those peaks at the higher binding energies of Y3$d_{5/2}$ and Y3$d_{3/2}$ at 159.55 and 161.60 eV correspond to the Y–F bonding. Fluorination was also confirmed at the peak of F1*s* located at 685.1 eV in the XPS spectrum of fluorine bonding. The peak position of the YOF coating was changed less than those of the Al_2O_3 bulk and Y_2O_3 coating after the plasma etching. The shift of the peaks of fluorine bonding to higher binding energy than those of oxygen bonding was attributed to the replacement of oxygen atoms by fluorine atoms around the cations during the etching process [26]. Fluorine bonding being stronger than oxygen bonding comes from the higher electronegativity of fluorine—3.98 as compared to 3.44 for oxygen [26].

The relative intensity ratio of the Al–F to Al–O peaks on the Al_2O_3 surface was 0.19 and that of the Y–F to Y–O peaks on the Y_2O_3 coating was 2.70, whereas that of the Y–F to Y–O peaks on the YOF coating surface was 4.79. These values indicate that the YOF coating formed much stronger fluorination on the surface, which would be related with the excellent intrinsic chemical stability and strong erosion resistance, suppressing the generation of fluorine contamination particles after exposure to fluorocarbon plasma.

Figure 8 shows the XPS depth profiles of compositions as a function of the Ar^+ sputtering time from the surface of the Al_2O_3, Y_2O_3, and YOF samples after exposure to CHF_3/Ar plasma for 60 min. Fluorination was confirmed on all the surfaces of the Al_2O_3, Y_2O_3, and YOF, while the fluorine content on the fluorinated layer of the YOF coating was higher than those of the Al_2O_3 and Y_2O_3. The percentages of F atoms reached the maximum values of 58.97% on the fluorinated layer of the Y_2O_3 coating (Figure 8b) and 17.76% on the Al_2O_3 bulk (Figure 8a), while the percentage reached the highest

value of 67.75% on the YOF coating surface (Figure 8c). Furthermore, the percentage of F atoms started to decrease from the maximum value to the original composition with sputtering time. Given that the fluorine content decreased from 17.76% and approached 0% with sputtering time in Figure 8a, the Al_2O_3 bulk surface appeared to be barely fluorinated. In addition, the fluorine content on the Y_2O_3 coating surface was rapidly decreased compared to that on the YOF coating surface (Figure 8b,c). These results indicated that the fluorination layer of the YOF coating was much thicker than that of the Y_2O_3 coating. This fluorination layer, with a higher concentration of fluorine on the surface, plays an important role in preventing erosion from fluorocarbon plasma and would not easily vaporize because of its chemical stability during the etching process [1,27].

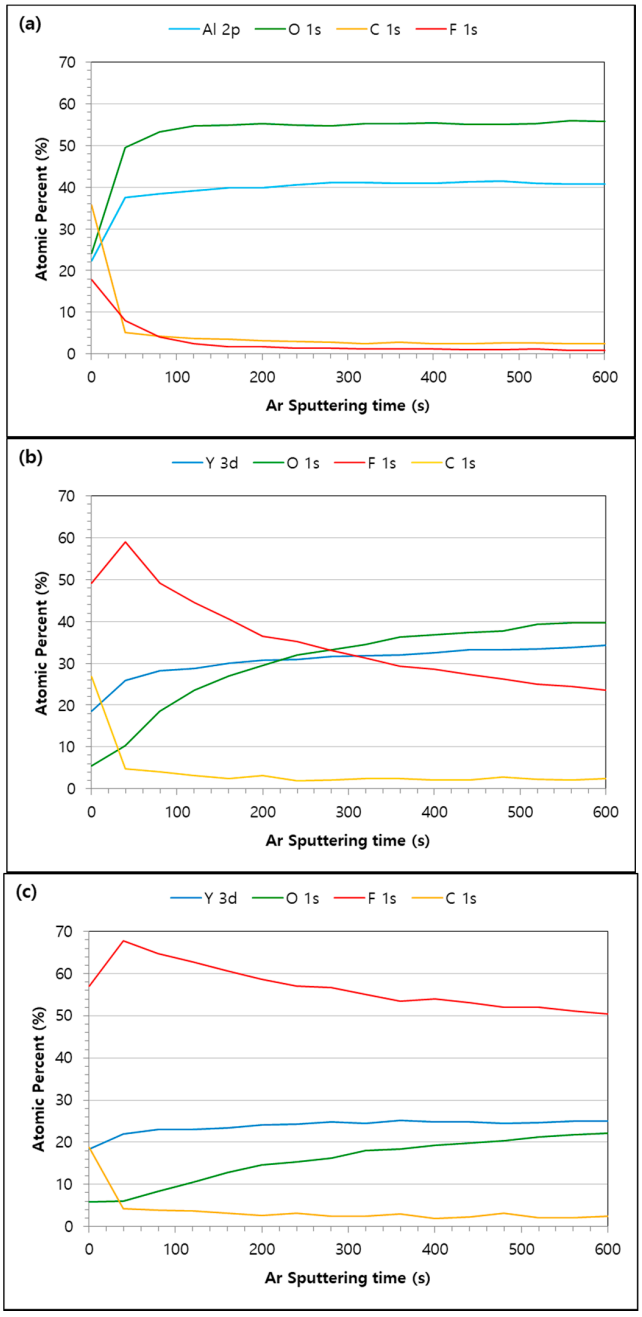

Figure 8. Variations of chemical compositions measured by XPS with the Ar sputtering time for (**a**) Al_2O_3 bulk, (**b**) Y_2O_3 coating, and (**c**) YOF coating after exposure to CHF_3/Ar plasma for 60 min.

On the other hand, the carbon content sharply decreased from the surface to the depth direction with the sputtering time in all of the Al_2O_3, Y_2O_3, and YOF samples, which indicated that the fluorocarbon layer is very thin, as shown in Figure 8. The thin fluorocarbon layer formed on the surface of the samples was previously reported in Si-based materials etched after exposure to fluorocarbon plasma [28]. From these results, we could confirm that the fluorination layer of the YOF coating was much thicker than those of the Al_2O_3 and Y_2O_3 samples. This would be why the YOF coating exhibits excellent plasma-resistance to CHF_3/Ar plasma etching.

4. Conclusions

The plasma etching behavior of the YOF coating deposited by SPS was studied using inductively coupled CHF_3/Ar plasma in comparison with those of Al_2O_3 bulk and Y_2O_3 coating. When the Al_2O_3 bulk and Y_2O_3 coating were exposed to fluorocarbon plasma, crater-like erosion sites and cavities were formed on the whole surface. In the case of the YOF coating, however, there was no obvious difference of the surface before and after the plasma etching. The etched depth of the Al_2O_3 bulk was about 3.5 times deeper than that of the Y_2O_3 coating, and the etched depth of the Y_2O_3 coating was about twice that of the YOF coating. Such high erosion resistance of the YOF coating to fluorocarbon plasma comes from the formation of a strongly fluorinated layer on the surface. The YOF coating deposited by SPS is expected to minimize the generation of contamination particles by preventing erosion of the inner wall of the semiconductor process chamber by fluorocarbon plasma.

Author Contributions: Conceptualization, S.L.; data curation, S.L.; formal analysis, S.L., J.L., and W.K.; funding acquisition, N.-M.H.; investigation, S.L., J.L., W.K., and N.-M.H.; methodology, S.L. and J.L.; project administration, W.K. and N.-M.H.; supervision, W.K. and N.-M.H.; writing—original draft, S.L. and W.K.; writing—review and editing, S.L., W.K., and N.-M.H. All authors have read and agreed to the published version of the manuscript.

Funding: This research was supported by the National Research Foundation of Korea (NRF) grant funded by the Korea government (MSIT) (No. 2020R1A5A6017701) and Samsung Electronics Co., Ltd.

Conflicts of Interest: The authors declare no conflict of interest.

References

1. Kim, D.-M.; Oh, Y.-S.; Kim, S.; Kim, H.-T.; Lim, D.-S.; Lee, S.-M. The erosion behaviors of Y_2O_3 and YF_3 coatings under fluorocarbon plasma. *Thin Solid Film.* **2011**, *519*, 6698–6702. [CrossRef]
2. Doemling, M.; Rueger, N.; Oehrlein, G.; Cook, J. Photoresist erosion studied in an inductively coupled plasma reactor employing CHF_3. *J. Vac. Sci. Technol. B Microelectron. Nanometer Struct. Process. Meas. Phenom.* **1998**, *16*, 1998–2005. [CrossRef]
3. Ito, N.; Moriya, T.; Uesugi, F.; Matsumoto, M.; Liu, S.; Kitayama, Y. Reduction of particle contamination in plasma-etching equipment by dehydration of chamber wall. *Jpn. J. Appl. Phys.* **2008**, *47*, 3630. [CrossRef]
4. Fukumoto, H.; Fujikake, I.; Takao, Y.; Eriguchi, K.; Ono, K. Plasma chemical behaviour of reactants and reaction products during inductively coupled CF_4 plasma etching of SiO_2. *Plasma Sources Sci. Technol.* **2009**, *18*, 045027. [CrossRef]
5. Blain, M.; Tipton, G.; Holber, W.; Selwyn, G.; Westerfield, P.; Maxwell, K. Particle behaviour in an electron cyclotron resonance plasma etch tool. *Plasma Sources Sci. Technol.* **1994**, *3*, 325. [CrossRef]
6. Tezani, L.; Pessoa, R.; Maciel, H.; Petraconi, G. Chemistry studies of SF_6/CF_4, SF_6/O_2 and CF_4/O_2 gas phase during hollow cathode reactive ion etching plasma. *Vacuum* **2014**, *106*, 64–68. [CrossRef]
7. Kim, D.-P.; Yeo, J.-W.; Kim, C.-I. Etching properties of Al_2O_3 films in inductively coupled plasma. *Thin Solid Film.* **2004**, *459*, 122–126. [CrossRef]
8. Miwa, K.; Takada, N.; Sasaki, K. Fluorination mechanisms of Al_2O_3 and Y_2O_3 surfaces irradiated by high-density CF_4/O_2 and SF_6/O_2 plasmas. *J. Vac. Sci. Technol. A Vac. Surf. Film.* **2009**, *27*, 831–835. [CrossRef]
9. Shiba, Y.; Teramoto, A.; Goto, T.; Kishi, Y.; Shirai, Y.; Sugawa, S. Stable yttrium oxyfluoride used in plasma process chamber. *J. Vac. Sci. Technol. A Vac. Surf. Film.* **2017**, *35*, 021405. [CrossRef]
10. Tsunoura, T.; Yoshida, K.; Yano, T.; Kishi, Y. Fabrication, characterization, and fluorine-plasma exposure behavior of dense yttrium oxyfluoride ceramics. *Jpn. J. Appl. Phys.* **2017**, *56*, 06HC02. [CrossRef]

11. Lee, J.; Lee, S.; Han, H.N.; Kim, W.; Hwang, N.-M. Yttrium oxyfluoride coatings deposited by suspension plasma spraying using coaxial feeding. *Coatings* **2020**, *10*, 481. [CrossRef]
12. Kim, D.-M.; Jang, M.-R.; Oh, Y.-S.; Kim, S.; Lee, S.-M.; Lee, S.-H. Relative sputtering rates of oxides and fluorides of aluminum and yttrium. *Surf. Coat. Technol.* **2017**, *309*, 694–697. [CrossRef]
13. Cao, Y.-C.; Zhao, L.; Luo, J.; Wang, K.; Zhang, B.-P.; Yokota, H.; Ito, Y.; Li, J.-F. Plasma etching behavior of Y_2O_3 ceramics: Comparative study with Al_2O_3. *Appl. Surf. Sci.* **2016**, *366*, 304–309. [CrossRef]
14. L Marqués, J.; Forster, G.; Schein, J. Multi-electrode plasma torches: Motivation for development and current state-of-the-art. *Open Plasma Phys. J.* **2009**, *2*, 89–98. [CrossRef]
15. Lee, J.-k.; Park, S.-J.; Oh, Y.-S.; Kim, S.; Kim, H.; Lee, S.-M. Fragmentation behavior of Y_2O_3 suspension in axially fed suspension plasma spray. *Surf. Coat. Technol.* **2017**, *309*, 456–461. [CrossRef]
16. Rueden, C.T.; Schindelin, J.; Hiner, M.C.; DeZonia, B.E.; Walter, A.E.; Arena, E.T.; Eliceiri, K.W. ImageJ2: ImageJ for the next generation of scientific image data. *BMC Bioinform.* **2017**, *18*, 529. [CrossRef]
17. Curry, N.; VanEvery, K.; Snyder, T.; Susnjar, J.; Bjorklund, S. Performance testing of suspension plasma sprayed thermal barrier coatings produced with varied suspension parameters. *Coatings* **2015**, *5*, 338–356. [CrossRef]
18. Lin, T.-K.; Wuu, D.-S.; Huang, S.-Y.; Wang, W.-K. Preparation and characterization of sprayed-yttrium oxyfluoride corrosion protective coating for plasma process chambers. *Coatings* **2018**, *8*, 373. [CrossRef]
19. Biqiu, L.; Lisha, L.; Kai, G.; Jiao, W.; Linlin, Z.; Zhang, H.; Wen, W.; Tieying, Y.; Jingtai, Z. Synthesis, characterization and luminescent properties of needle-like lanthanide-doped orthorhombic $Y_5O_4F_7$. *J. Rare Earths* **2013**, *31*, 745–749.
20. Park, S.-J.; Kim, H.; Lee, S.-M. Solid-state synthesis of yttirum oxyfluoride powders and their application to suspension plasma spray coating. *Korean J. Mater. Res.* **2017**, *27*, 710–715. [CrossRef]
21. Ashizawa, H.; Yoshida, K. Effect of the microstructures of yttria ceramics on their plasma corrosion behavior. *Ceram. Int.* **2019**, *45*, 0272–8842. [CrossRef]
22. Wagner, C.D.; Riggs, W.M.; Davis, L.E.; Moulder, J.F. *Handbook of X-ray Photoelectron Spectroscopy*; Muilenberg, G.E., Ed.; Perkin-Elmer Corporation: Minnesota, MN, USA, 1979.
23. Fundamental XPS Data to Assist Peak-Fitting. Available online: http://srdata.nist.gov/ (accessed on 11 August 2020).
24. Diehl, R.; Brandt, G. Crystal structure refinement of $YAlO_3$, a promising laser material. *Mater. Res. Bull.* **1975**, *10*, 85–90. [CrossRef]
25. Pei, L.; Jiapi, Z.; Yuankun, Z.; Jiecai, H. Preparation and optical properties of sputtered-deposition yttrium fluoride film. *Nucl. Instrum. Methods Phys. Res. Sect. B* **2013**, *307*, 429–433. [CrossRef]
26. Zhong, H.X.; Hong, J.M.; Cao, X.F.; Chen, X.T.; Xue, Z.L. Ionic-liquid-assisted synthesis of YF_3 with different crystalline phases and morphologies. *Mater. Res. Bull.* **2009**, *44*, 623–628. [CrossRef]
27. Lin, T.-K.; Wang, W.-K.; Huang, S.-Y.; Tasi, C.-T.; Wuu, D.-S. Comparison of erosion behavior and particle contamination in mass-production CF_4/O_2 plasma chambers using Y_2O_3 and YF_3 protective coatings. *Nanomaterials* **2017**, *7*, 183. [CrossRef] [PubMed]
28. Standaert, T.E.F.M.; Hedlund, C.; Joseph, E.A.; Oehrlein, G.S.; Dalton, T.J. Role of fluorocarbon film formation in the etching of silicon, silicon dioxide, siliconnitride, and amorphous hydrogenated silicon carbide. *J. Vac. Sci. Technol. A* **2004**, *22*, 53–60. [CrossRef]